Alfvén Turbulence Driven by High-Dimensional Interior Crisis in the Solar Wind

A. C.-L. Chian[*,†], E. L. Rempel[*,†], E. E. N. Macau[†], R. R. Rosa[†] and F. Christiansen[**]

[*]*World Institute for Space Environment Research-WISER, NITP, University of Adelaide, SA 5005, Australia*
[†]*National Institute for Space Research-INPE, P.O. Box 515, 12227-010 São José dos Campos, SP, Brazil*
[**]*Solar-Terrestrial Physics Division, Danish Meteorological Institute, Lyngbyvej 100, DK-2100 Copenhagen, Denmark*

Abstract. Alfvén intermittent turbulence has been observed in the solar wind. It has been previously shown that the interplanetary Alfvén intermittent turbulence can appear due to a low-dimensional temporal chaos [1]. In this paper, we study the nonlinear spatiotemporal dynamics of Alfvén waves governed by the Kuramoto-Sivashinsky equation which describes the phase evolution of a large-amplitude Alfvén wave. We investigate the Alfvén turbulence driven by a high-dimensional interior crisis, which is a global bifurcation caused by the collision of a chaotic attractor with an unstable periodic orbit. This nonlinear phenomenon is analyzed using the numerical solutions of the model equation. The identification of the unstable periodic orbits and their invariant manifolds is fundamental for understanding the instability, chaos and turbulence in complex systems such as the solar wind plasma. The high-dimensional dynamical system approach to space environment turbulence developed in this paper can improve our interpretation of the origin and the nature of Alfvén turbulence observed in the solar wind.

INTRODUCTION

In a recent paper by Chian, Borotto and Gonzalez [1], Alfvén turbulence driven by a low-dimensional chaos in the solar wind was studied. Through a numerical analysis of the stationary solutions of the driven-dissipative nonlinear Schrödinger equation, two types of interplanetary Alfvén intermittency were identified: type-I Pomeau-Manneville intermittency and interior crisis-induced intermittency. The nonlinear Schrödinger equation and the derivative nonlinear Schrödinger equation have also been used to model the propagation of finite-amplitude Alfvén waves [2, 3] and the formation of magnetic holes [4] in the solar wind, as well as the solar corona heating [5]. The spatiotemporal chaos of Alfvén waves appears in a system of MHD coupled wave equations that are the generalization of the nonlinear Schrödinger equation [6].

It was demonstrated by Lefebvre and Hada [7] that under the assumption of weak instability and wave-packet limit the derivative nonlinear Schrödinger equation, that describes the modulational instability of quasi-parallel Alfvén waves of moderate amplitudes in a finite β plasma, reduces to a complex Ginzburg-Landau equation. In this paper, we study the spatiotemporal dynamics of a nonlinear Alfvén wave in the solar wind governed by the Kuramoto-Sivashinsky equation, which under certain approximations describes the phase evolution of the complex amplitude of the Ginzburg-Landau equation.

THE KURAMOTO-SIVASHINSKY EQUATION

The one-dimensional Kuramoto-Sivashinsky equation can be written as [8]

$$\partial_t u = -\partial_x^2 u - \nu \partial_x^4 u - \partial_x u^2, \tag{1}$$

where ν is a 'viscosity' damping parameter. We assume that $u(x,t)$ is subject to periodic boundary conditions $u(x,t) = u(x+2\pi,t)$ and expand the solutions in a discrete spatial Fourier series

$$u(x,t) = \sum_{k=-\infty}^{\infty} b_k(t)e^{ikx}. \tag{2}$$

Substituting Eq. (2) into Eq. (1) yields an infinite set of ordinary differential equations for the complex Fourier coefficients $b_k(t)$

$$\dot{b}_k(t) = (k^2 - \nu k^4)b_k(t) - ik \sum_{m=-\infty}^{\infty} b_m(t)b_{k-m}(t), \tag{3}$$

where the dot denotes derivative with respect to t. Reality of $u(x,t)$ implies that $b_{-k} = b_k^*$. We restrict our investigation to the subspace of odd functions $u(x,t) = -u(-x,t)$ assuming that $b_k(t)$ are purely imaginary by setting $b_k(t) = -ia_k(t)/2$, where $a_k(t)$ are real. Equation (3) then becomes

$$\dot{a}_k(t) = (k^2 - \nu k^4)a_k(t) - \frac{k}{2}\sum_{m=-\infty}^{\infty} a_m(t)a_{k-m}(t), \quad (4)$$

where $a_0 = 0$, $1 \leq k \leq N$, N is the truncation order. We integrate the high-dimensional dynamical system given by Eq. (4) using a fourth-order variable step Runge-Kutta integration routine. We choose $N = 16$, since numerical tests indicate that for the range of the control parameter ν used in this paper the solution dynamics remains essentially unaltered for $N > 16$. In all the computational results presented in this paper, higher order truncations yield the same numerical conclusions as the 16-mode truncation. We adopt a Poincaré map with the $(N-1)$ dimensional hyperplane defined by $a_1 = 0$, with $\dot{a}_1 > 0$.

Nonlinear Dynamical Analysis

A bifurcation diagram can be obtained from the numerical solutions of the 16-mode truncation of Eq. (4) by varying the control parameter ν and plotting the Poincaré points of one Fourier mode after discarding the initial transient. Figure 1a shows a period-3 (p-3) window where we plot the Poincaré points of the Fourier mode a_6 as a function of ν. The corresponding behavior of the maximum Lyapunov exponent is shown in Fig. 1b. Evidently, the high-dimensional temporal dynamics of the K-S equation preserves the typical dynamical features of a low-dimensional dynamical system. The dotted lines in Fig. 1a denote the Poincaré points of the p-3 unstable periodic orbit (UPO) which emerges via a saddle-node bifurcation at $\nu = 0.02992498$, marked SN in Fig. 1a. In this paper, we will analyze the role played by this p-3 UPO in the onset of interior crisis at $\nu_{IC} = 0.02992021$, marked IC in Fig. 1.

The interior crisis at ν_{IC} occurs when the p-3 UPO collides head on with the 3-band weak strange attractor evolved from a cascade of period-doubling bifurcations, as seen in Fig. 1a.

The interior crisis leads to a sudden expansion of a strange attractor, turning the weak strange attractor (WSA) into a strong strange attractor (SSA), as seen in Fig. 2. Figure 2 is a 3-dimensional projection (a_1, a_{10}, a_{16}) of the strong strange attractor (light line) defined in the 15-dimensional Poincaré hyperplane right after the crisis ($\nu = 0.02992020$), superimposed by the 3-band weak strange attractor (dark line) at crisis
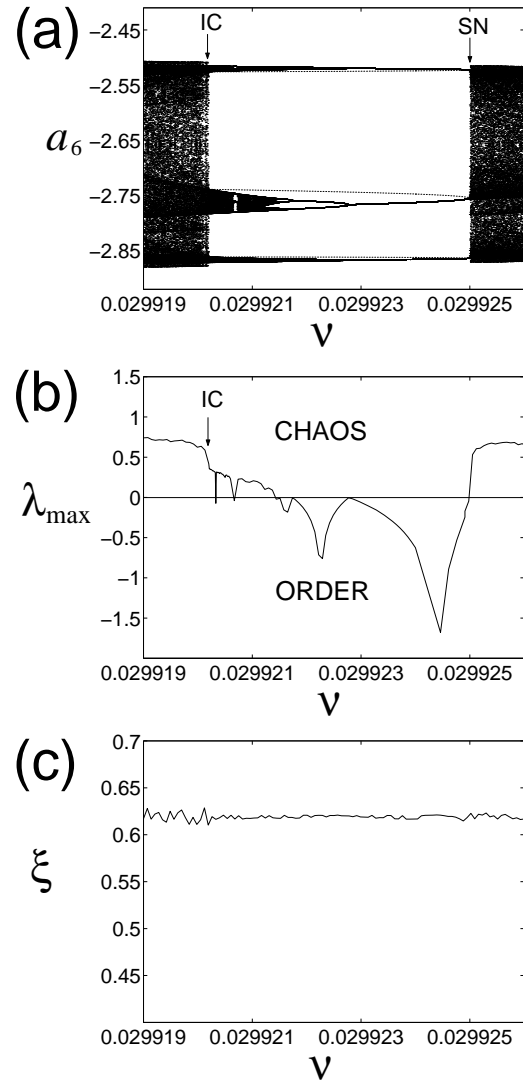

FIGURE 1. (a) Bifurcation diagram of a_6 as a function of ν. IC denotes interior crisis and SN denotes saddle-node bifurcation. The dotted lines represent a period-3 unstable periodic orbit. (b) Variation of the maximum Lyapunov exponent λ_{max} with ν. (c) Variation of the correlation length σ with ν.

($\nu = 0.02992021$). The abrupt increase in the system's chaoticity after the interior crisis can be characterized by the value of the maximum Lyapunov exponent (λ_{max}), plotted in Fig. 1(b). At crisis ($\nu_{IC} = 0.02992021$), $\lambda_{max} = 0.35$, and after the crisis at $\nu = 0.02992006$, $\lambda_{max} = 0.62$. In Fig. 1(c) we plotted the spatial correlation length σ, which remains basically unaltered throughout the whole range of ν used in Fig. 1. This means that there is little variance in the spatial disorder of the pattern. An inspection of the spatiotemporal pattern $u(x,t)$ after the crisis ($\nu = 0.02992006$), shown in Fig. 3, reveals that for the
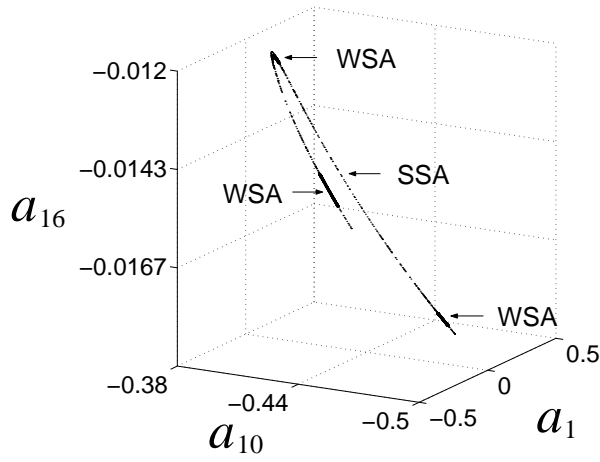
FIGURE 2. Three-dimensional projection (a_1, a_{10}, a_{16}) of the strong strange attractor SSA (light line) defined in the 15-dimensional Poincaré hyperplane right after crisis at $v = 0.02992020$, superimposed by the 3-band weak strange attractor WSA (dark line) at crisis $(v = 0.02992021)$.
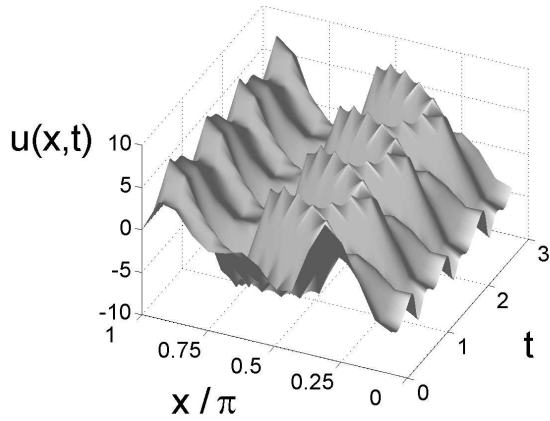

FIGURE 3. The spatiotemporal pattern of $u(x,t)$ after the crisis at $v = 0.02992006$. The system dynamics is chaotic in time but coherent in space.

chosen values of v and the spatial system size $L = 2\pi$, the dynamics of the Kuramoto-Sivashinsky equation is coherent in space.

On the Poincaré hyperplane an unstable periodic orbit turns into a saddle fixed point, with its associated invariant stable and unstable manifolds. At crisis, only one of the 16 stability eigenvalues of the p-3 UPO illustrated in Fig. 1a has an absolute value greater than 1. This implies that its invariant unstable manifold is a one-dimensional curve embedded in the 15-dimensional Poincaré space. Of the remaining eigenvalues, one has absolute value equal to unity and all the other fourteen have absolute values less than one, implying that the invariant stable
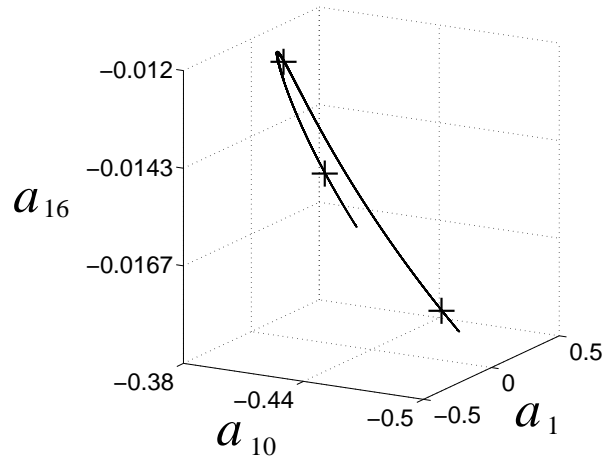

FIGURE 4. Three-dimensional projection (a_1, a_{10}, a_{16}) of the invariant unstable manifolds of the period-3 saddle (crosses) right after the crisis at $v = 0.02992020$.

manifolds have dimension fourteen. Although we have adopted a 16-mode truncated system in our analysis, all the calculations performed can be extended to an arbitrary high number $(N < \infty)$ of modes for an appropriate choice of v and L. Figure 4 is a plot of the projection of the invariant unstable manifold of the p-3 UPO onto three axes (a_1, a_{10}, a_{16}) at $v = 0.02992020$, right after the interior crisis. The crosses represent the p-3 UPO. The invariant unstable manifolds consist of infinitely many distinct, discrete Poincaré points whose backward orbits converge to the saddle.

We proceed next with the characterization of the high-dimensional crisis at v_{IC} by showing in Fig. 5 the collision of the weak strange attractor with the p-3 UPO in the reduced 2-dimensional Poincaré plane $(a_5 \text{ vs. } a_6)$, in the vicinity of the upper cross in Fig. 4. The dark line denotes the strange attractor, and the light line denotes the numerically computed invariant unstable manifold of the saddle periodic orbit. Figures 5a,b,c display the dynamics before, at, and after the crisis, respectively. Note that the strange attractor always "overlaps" the invariant unstable manifold. At the crisis point $v_{IC} = 0.02992021$, the chaotic attractor is the closure of one branch of the unstable manifold of the p-3 UPO, as seen in Fig. 5b. The "head-on" collision of the weak strange attractor with the p-3 UPO at v_{IC}, shown in Fig. 5b, proves the occurrence of an interior crisis. Although we are showing only two of the 16 modes, the collision can be seen in any choice of Fourier modes. This collision leads to an abrupt expansion of the strange attractor, as seen in Fig. 5c. A comparision of Figs. 2 and 4 confirms that, after the crisis, the strong strange attractor and the invariant unstable manifold "overlap" with each other.
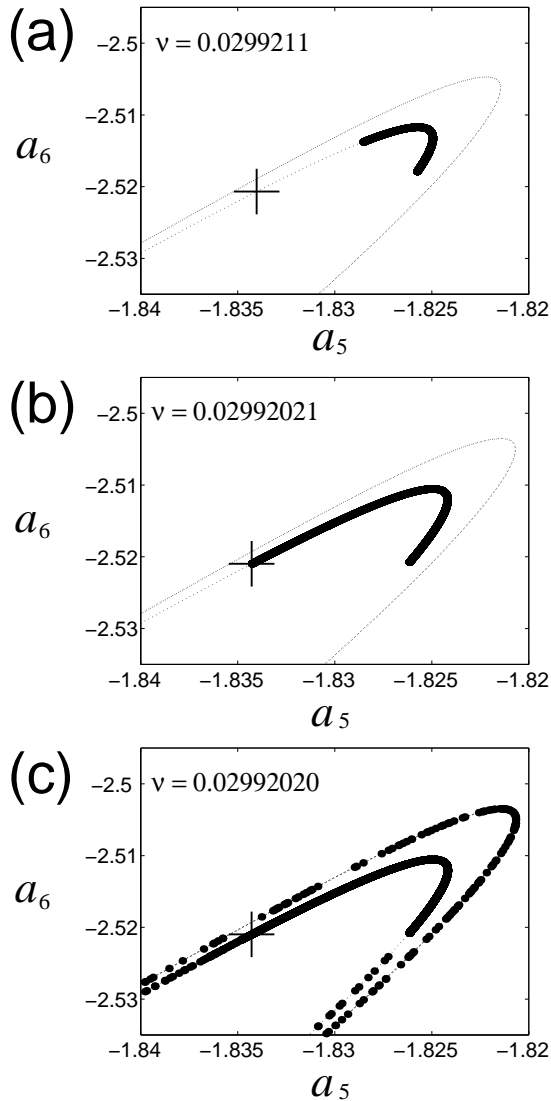
FIGURE 5. The plots of the strange attractor (dark line) and invariant unstable manifolds (light lines) of the saddle before (a), at (b) and after (c) crisis. The cross denotes one of the saddle points.

DISCUSSION

The high-dimensional interior crisis discussed in this paper can improve our understanding of Alfvén intermittent turbulence in the Solar wind. Observations of Alfvénic intermittent turbulence in the solar wind were reported by Marsch and Liu [9] and Tu and Marsch [10]. Using the *Helios 2* data in the inner solar wind between 0.3 and 1.0 AU, they identified the multifractal nature of interplanetary Alfvénic fluctuations and the dependence of Alfvénic intermittent turbulence on stream speed and radial distance from the Sun. It was shown by Chian, Borotto and Gonzalez [1] that an interior crisis can induce a temporal Alfvén intermittency, yielding a power-law spectrum similar to the typical power spectra of Alfvénic turbulence observed in the interplanetary medium. The present paper suggests that the spatiotemporal intermittency of interplanetary Alfvén waves can be driven by an interior crisis. There is observational evidence of Alfvén chaos in the solar wind. A nonlinear time series analysis of Alfvén waves in the low-speed streams of the solar wind detected by the Helios spacecraft in the inner heliosphere shows that the Lyapunov exponent and the entropy are positive, which indicates that the solar wind plasma is in a chaotic state [11].

REFERENCES

1. Chian, A. C.-L., Borotto, F. A., and Gonzalez, W. D., *Astrophys. J.*, **505**, 993-998 (1998).
2. Ghosh, S., and Papadopoulos, K., *Phys. Fluids*, **30**, 1371-1387 (1987).
3. Hada, T., Kennel, C. F., Buti, B., and Mjφlhus, E., *Phys. Fluids B*, **2**, 2581-2590 (1990).
4. Baumgartel, K., *J. Geophys. Res.*, **104**, 28295-28308 (1999).
5. Champeaux, S. et al., *Astrophys. J.*, **486**, 477-483 (1997).
6. Oliveira, L. P. L., Rizzato, F. B., and Chian, A. C.-L., *J. Plasma Phys.*, **58**, 441-453 (1997).
7. Lefebvre, B., and Hada, T. 'Spatiotemporal Behavior of a Driven System of MHD Waves", AGU Fall Meeting, San Francisco (2000).
8. Chian, A. C.-L., Rempel, E. L., Macau, E. E. N. Rosa, R. R., Christiansen, F., *Phys. Rev. E* **65**, 035203(R) (2002).
9. Marsch, E., Liu, S. *Ann. Geophys.*, **11**, 227 (1993).
10. Tu, C.-Y., Marsch, E., *Space Sci. Rev.*, **33**, 1 (1995).
11. Macek, W. M., and Redaelli, S., *Phys. Rev. E*, **62**, 6496-6504 (2000).